

# Journal of Intelligent Material Systems and Structures

<http://jim.sagepub.com/>

---

## **A refined shear lag model for adhesively bonded piezo-impedance transducers**

Suresh Bhalla and Sumedha Moharana

*Journal of Intelligent Material Systems and Structures* 2013 24: 33 originally published online 5 September 2012

DOI: 10.1177/1045389X12457837

The online version of this article can be found at:

<http://jim.sagepub.com/content/24/1/33>

---

Published by:



<http://www.sagepublications.com>

**Additional services and information for *Journal of Intelligent Material Systems and Structures* can be found at:**

**Email Alerts:** <http://jim.sagepub.com/cgi/alerts>

**Subscriptions:** <http://jim.sagepub.com/subscriptions>

**Reprints:** <http://www.sagepub.com/journalsReprints.nav>

**Permissions:** <http://www.sagepub.com/journalsPermissions.nav>

**Citations:** <http://jim.sagepub.com/content/24/1/33.refs.html>

>> [Version of Record](#) - Dec 18, 2012

[OnlineFirst Version of Record](#) - Sep 5, 2012

[What is This?](#)

# A refined shear lag model for adhesively bonded piezo-impedance transducers

Suresh Bhalla and Sumedha Moharana

*Journal of Intelligent Material Systems and Structures*  
24(1) 33–48  
© The Author(s) 2012  
Reprints and permissions:  
sagepub.co.uk/journalsPermissions.nav  
DOI: 10.1177/1045389X12457837  
jim.sagepub.com  


## Abstract

The performance (sensing/actuating) of a piezotransducer highly depends upon the ability of the bond layer to transfer the stress and strain (through shear lag mechanism) between the transducer and the structure. Therefore, the coupled electromechanical response of the piezotransducer should consider the effect of dynamic behaviour, geometry and composition of the adhesive layer used to bond the transducer patch on the structure. This article presents a new refined analytical model for inclusion of the shear lag effect in modelling of adhesively bonded piezoelectric ceramic (lead zirconate titanate) patches for consideration in the electromechanical impedance technique. The previous models neglected the inertial term in shear lag formulations for simplicity. The present refined model, on the other hand, considers the inertial and the shear lag effects simultaneously, and is therefore more rigorous and complete. In this article, the formulations are first derived for one-dimensional case, and then extended to two-dimensional lead zirconate titanate–structure interaction. The overall results are found to be in better proximity to experimental observations. The refined formulations are employed for a detailed stress analysis of the bond layer. The article concludes with a parametric study on the influence of various sensor parameters on the electromechanical impedance signatures.

## Keywords

Electromechanical impedance technique, adhesive bond, shear lag, conductance, susceptance, structural health monitoring, shear lag

## Introduction

This article derives a new refined analytical model for incorporating shear lag effect in adhesively bonded lead zirconate titanate (PZT) piezo-ceramic patches pertinent to the electromechanical impedance (EMI) technique. During the last two decades, the EMI technique has emerged as a competitive and prospective technique for structural health monitoring (SHM) and non-destructive evaluation (NDE) for wide spectrum of structures (Ayres et al., 1998; Bhalla and Soh, 2004a, 2004b; Lim et al., 2006; Park et al., 2006; Shanker et al., 2011; Soh et al., 2000). In this technique, a surface-bonded PZT patch captures the structural dynamic information of the host structure in the form of admittance signature (comprising of conductance, the real part, and susceptance, the imaginary part), over a pre-set frequency range running from few tens of kilohertz to few hundreds of kilohertz (generally between 30 and 400 kHz). Any damage to the structure, even if highly incipient in nature, alters the admittance signature discernibly, thereby enabling its timely detection. Over the last one and half decades, the technique has established

its potential as a viable high-resolution damage diagnosis technique, driven by active theoretical research and development of low-cost hardware adaptations (Bhalla et al., 2009a; Overly et al., 2008). The adhesive bond forms an interfacial layer of finite thickness between the patch and host structure. The adhesive does not change the material properties of adherents, and attaching the PZT patches using adhesives enables a broader range of applications than other bondings (Wang and Zeng, 2008). The mechanical and geometrical properties of the adhesive bond layer affect the overall performance of the PZT–structure interaction model (Dugani, 2009).

The working of the EMI technique can be described by following governing equation derived by Liang et al.

---

Department of Civil Engineering, Indian Institute of Technology Delhi, New Delhi, India

### Corresponding author:

Suresh Bhalla, Department of Civil Engineering, Indian Institute of Technology Delhi, Hauz Khas, New Delhi 110016, India.  
Email: sbhalla@civil.iitd.ac.in

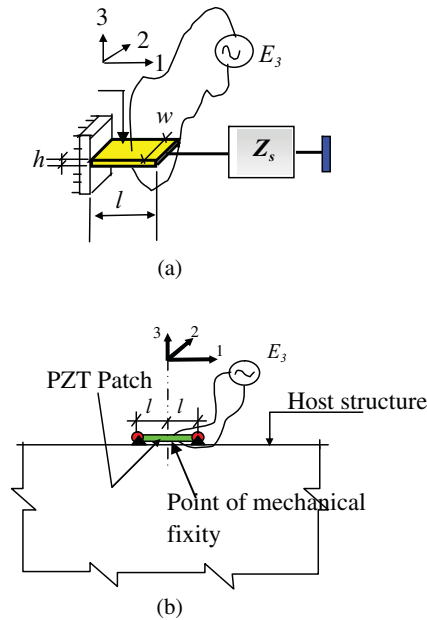


**Figure 1.** (a) Liang's 1D impedance model. (b) A PZT patch surface bonded to the structure. ID: one-dimensional; PZT: lead zirconate titanate.

(1994) for a PZT patch bonded to one-dimensional (1D) structure, as shown in Figure 1

$$\bar{Y} = 2\omega \frac{wl}{h_p} \left[ \frac{1}{(\epsilon_{33}^T - d_{31}^2)} + \left( \frac{Z_a}{Z_s + Z_a} \right) d_{31}^2 \bar{Y}^E \left( \frac{\tan kl}{kl} \right) \right] \quad (1)$$

where  $\bar{Y}$  is the complex electromechanical admittance,  $\omega$  is the angular frequency,  $w$  is the width of the patch,  $l$  is the half length,  $h_p$  is the thickness,  $\frac{1}{\epsilon_{33}^T} = \epsilon_{33}^T (1 - \delta j)$  is the complex piezoelectric permittivity ( $\delta$  being the dielectric loss factor),  $\bar{Y}^E = Y^E (1 + \eta j)$  is the complex Young's modulus ( $\eta$  being the mechanical loss factor),  $Z_a$  is the mechanical impedance of the PZT patch,  $Z_s$  is the mechanical impedance of the host structure and  $k$  is the wave number. This equation couples  $Z_s$  (mechanical impedance of the structure) to the electromechanical admittance  $\bar{Y}$ , which means that any damage to the structure (change of  $Z_s$ ) will reflect itself as change in  $\bar{Y}$ , thereby providing indication of the damage.

The main limitation of Liang's model, however, is that it considers the PZT patch to be connected to the structure at its ends only (Figure 1(b)) and ignores the presence of the adhesive as the bond layer. On the other hand, in actual PZT-structure system, where a finitely thick bond layer connects the PZT patch to the structure, the force/strain transfer takes places as illustrated in Figure 2, with the bond layer undergoing shear deformation. As a result, if the PZT patch is employed as an actuator, the deformation on the surface of the structure is lesser than that at the end of the patch (i.e. referring to Figure 2,  $u_o < u_{po}$ ).

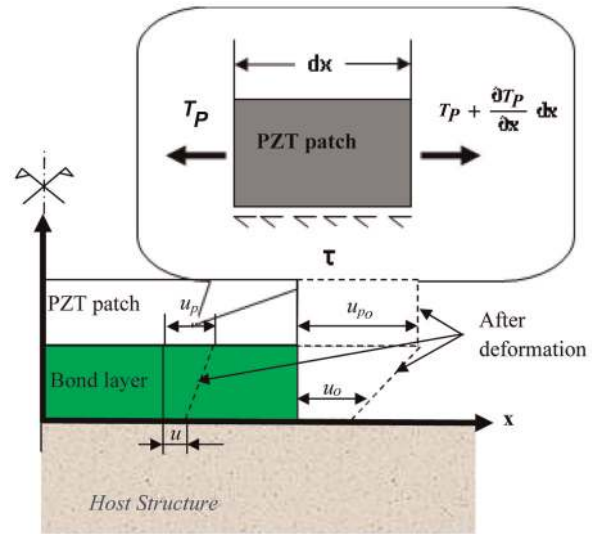


**Figure 2.** Force and strain transfer mechanism through adhesive bond layer. PZT: lead zirconate titanate.

Similarly, when used as a sensor, strain on the surface of the host structure is not fully transferred to the PZT patch. Considering the dynamic equilibrium of an infinitesimally small element of the PZT patch and the bond layer, following differential equation relates the mass with the axial and the shear stresses (Bhalla and Soh, 2004c)

$$\tau w dx + (dm) \frac{\partial^2 u_p}{\partial t^2} = \frac{\partial T_p}{\partial x} h_p w dx \quad (2)$$

where  $u_p$  is the displacement in the PZT patch,  $dm$  is the mass of the infinitesimal element,  $\tau$  is the interfacial shear stress and  $T_p$  is the axial stress in the PZT patch. Liang's impedance formulation (equation (1)) ignores the shear term and assumes that the structure, represented by impedance  $Z_s$ , is connected to the PZT patch at the two ends, as illustrated in Figure 1(b).

Crawley and De Luis (1987) analytically modelled the actuation of a beam element by an adhesively bonded PZT patch. Sirohi and Chopra (2000) derived similar formulations for piezoelectric elements (ceramic or polymer) employed as strain sensors on beams. In both cases, the governing factor, called shear lag parameter  $\Gamma$ , was mathematically expressed as

$$\Gamma = \sqrt{\frac{G_s}{Y_p h_p h_s} + \frac{3G_s w_p}{Y_b w_b h_b h_p}} \quad (3)$$

where  $G_s$  is the shear modulus of the adhesive;  $Y_b$  is the Young's modulus of elasticity of the beam;  $h_s$  and  $h_p$  are the thicknesses of the adhesive layer and the PZT patch, respectively;  $w_b$  is the width of the beam and  $w_p$  is the width of the patch. Based on the analysis

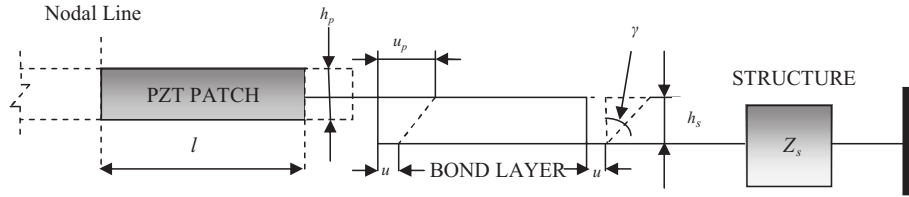


**Figure 3.** Simplified 1D impedance model (Bhalla et al., 2009b). ID: one-dimensional; PZT: lead zirconate titanate.

presented by Crawley and De Luis (1987) and Sirohi and Chopra (2000), the shear lag effect can be deemed negligible if the condition  $\Gamma < 30 \text{ cm}^{-1}$  is satisfied for which case, the force is effectively transferred over the end regions of the PZT patch. However, for  $\Gamma < 30 \text{ cm}^{-1}$ , it is not reasonable to ignore shear lag effect.

As far as the EMI technique is concerned, where the same patch serves as the sensor and the actuator simultaneously, understanding of the shear lag effect is much more important (Abe et al., 2002). For the EMI technique, Xu and Liu (2002) proposed a model that considered the bond layer as a single-degree-of-freedom system. Ong et al. (2002) partially included shear lag effect by incorporating the effective length parameter suggested by Sirohi and Chopra (2000) for sensor case (however, ignoring the actuator effect). Bhalla and Soh (2004c) were the first to realistically integrate the shear lag effect in the EMI technique considering both sensor and actuator effects simultaneously. However, they simplified equation (2) by ignoring the inertia term  $(dm)\ddot{u}_p$ . Equation (2) was combined with another equation adopted from the definition of mechanical impedance, that is

$$F = T_p w h_p = -Z_s j \omega u \quad (4)$$

where  $Z_s$  is the mechanical impedance of the structure and  $u$  is the host structure's displacement. The combination of the two equations (equations (2) and (4)) resulted in a fourth-order differential equation, which was solved for  $u$  and  $u_p$ . The equivalent mechanical impedance (incorporating the shear lag effect) was then obtained as

$$Z_{eq} = Z_s \frac{u(x=l)}{u_p(x=l)} = \frac{Z_s}{\left(1 + \frac{u'_o}{u_o \bar{p}}\right)} \quad (5)$$

where  $u_o$  is the end displacement (as shown in Figure 2),  $u'_o$  is the edge strain and  $\bar{p}$  is the shear lag parameter, defined by

$$\bar{p} = -\frac{w \overline{G_s}}{Z_s h_s j \omega} \quad (6)$$

where  $\overline{G_s} = G_s(1 + \eta'j)$ ,  $\eta'$  being the mechanical loss factor of the bond layer. The model was thereafter extended to the 2D case, and the resulting analytical

expression was validated with experimental data. Useful interpretations as well as parametric studies were arrived at based on the developed model. The predictions of the model were independently experimentally verified by Qing et al. (2006). However, as pointed above, this model ignored the inertia effect. In addition, strictly speaking, equation (4) is not valid at the ends of the PZT patch, which are stress free (Crawley and De Luis, 1987), thus introducing additional error over and above due to the negligence of the inertia term.

Bhalla et al. (2009b) derived an alternate simplified shear lag model wherein the adhesive bond layer was assumed to be connected between the PZT patch and host structure, such that it transferred the force between the two through pure shear mechanism, as illustrated in Figure 3. For this particular mechanism, the equivalent structural impedance  $Z_{s,eq}$  was derived as

$$Z_{s,eq} = \frac{Z_s}{\left[1 - \left(\frac{Z_s \omega h_s j}{2l^2 G_s}\right)\right]} \quad (7)$$

The particular advantage of the simplified model is its ability in solving the inverse problem, that is, obtaining the true structural mechanical impedance from the measured admittance signature, thus eliminating the bond layer's contribution. The model, when extended to 2D, yielded results satisfactorily matching with those of earlier model (Bhalla and Soh, 2004c).

This article presents the development of a new refined analytical model duly considering the inertia effect (inertia term of equation (2)), ignored in the previous models. Furthermore, the effects of the mass of the adhesive bond layer are also separately included. In place of using equation (4), the new refined model makes use of shear force transfer mechanism to arrive at the second necessary equation, which is more accurate. The next section presents a step-by-step derivation of the refined model for 1D followed by its extension to 2D and consideration of additional effects such as adhesive layer's mass, parametric study and comparison with previous models.

## 1D refined shear lag formulations

The refined model presented in this article rigorously considers the inertial term of equation (2) that was

neglected in the previous model of Bhalla and Soh (2004c). Making substitution for following terms in equation (2)

$$dm = \rho wh_p dx \quad (8a)$$

$$\ddot{u}_p = -\omega^2 u_p \quad (8b)$$

$$T_p = \overline{Y^E}(u'_p - \Lambda) \quad (8c)$$

and

$$\tau = \frac{\overline{G_s}(u_p - u)}{h_s} \quad (8d)$$

where  $\rho$  is the density of the PZT patch,  $\Lambda = d_{31}E_3$  is the free piezoelectric strain and  $\overline{G_s}$  is the complex shear modulus of elasticity of the adhesive bond layer, the equation can be reduced to a compact form as

$$\bar{\alpha}u_p - u = \frac{1}{q}u_p'' \quad (9)$$

where

$$\bar{\alpha} = 1 - \frac{\rho h_p h_s \omega^2}{\overline{G_s}} \quad (10a)$$

and

$$q = \frac{\overline{G_s}}{\overline{Y^E} h_s h_p} \approx \frac{G_s}{Y^E h_s h_p} \quad (10b)$$

Here,  $\bar{\alpha}$  can be termed as the inertia parameter. In the previous model (Bhalla and Soh, 2004c), a value of unity was considered for  $\bar{\alpha}$ . Bhalla and Soh (2004a) derived the second necessary equation by considering equilibrium of forces at a vertical section passing through the PZT patch, as given by equation (4), which basically equates the axial force in the PZT patch (negative sign implies compression) with the product of mechanical impedance and velocity (note that  $\dot{u} = j\omega u$ ). It is assumed herein that  $Z_s$  is constant over the entire length of the PZT patch, due to its being infinitesimally small as compared to the host structure. This equation however, is not satisfied at the ends of the PZT patch, where  $T_1 = 0$ , as imposed by the boundary conditions that the ends of the PZT patch are stress free.

In this article, however, the second equation is derived from the shear stress transfer mechanism illustrated in Figure 4, which shows the portion of the PZT patch between coordinates 0 and  $x$ . Equating the shear force transferred between these two coordinates to the force-impedance relation, we can write

$$\int_x^l \tau w dx = Z_s j \omega u \quad (11)$$

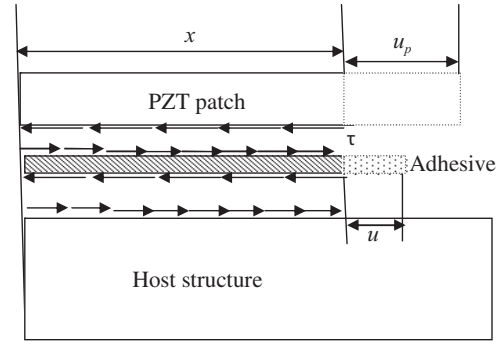


**Figure 4.** Shear transfer mechanism through bond layer. PZT: lead zirconate titanate.

or

$$\int_x^l \frac{w \overline{G_s}(u_p - u) dx}{h_s} = Z_s j \omega u \quad (12)$$

Differentiating both sides with respect to  $x$ , we get

$$-\frac{w \overline{G_s}(u_p - u)}{h_s} = Z_s j \omega u' \quad (13)$$

which can be simplified to

$$u_p = u + \frac{u'}{\bar{p}} \quad (14)$$

where  $\bar{p}$  is the shear lag parameter defined by equation (6). Equations (9) and (14) are the governing shear lag equations for the new model, with the shear lag parameters  $\bar{p}$  and  $q$  same as in the previous model (Bhalla and Soh, 2004c). Differentiating equation (14) twice with respect to  $x$ , we get

$$u_p'' = u'' + \frac{u'''}{\bar{p}} \quad (15)$$

Eliminating  $u_p$  and  $u_p''$  from equation (9), making the use of equations (14) and (15), we get the governing differential equation as

$$u'''' + \bar{p}u'' - \bar{\alpha}qu' + (1 - \bar{\alpha})\bar{p}qu = 0 \quad (16)$$

This is homogenous differential equation, whose characteristic equation is

$$\lambda^3 + \bar{p}\lambda^2 - \bar{\alpha}q\lambda + (1 - \bar{\alpha})\bar{p}q = 0 \quad (17)$$

The above equation is a polynomial equation with complex coefficients, whose roots  $\lambda_1$ ,  $\lambda_2$  and  $\lambda_3$  lead to following solution for  $u$ , the displacement on the surface of the host structure.

$$u = A_1 e^{\lambda_1 x} + A_2 e^{\lambda_2 x} + A_3 e^{\lambda_3 x} \quad (18)$$

where  $A_1$ ,  $A_2$  and  $A_3$  are constants to be determined from the boundary conditions. Differentiating equation (18) with respect to  $x$ , we get

$$u' = A_1\lambda_1 e^{\lambda_1 x} + A_2\lambda_2 e^{\lambda_2 x} + A_3\lambda_3 e^{\lambda_3 x} \quad (19)$$

Hence, from equation (14), an expression for  $u_p$  can be written as

$$u_p = A_1 \left(1 + \frac{\lambda_1}{\bar{P}}\right) e^{\lambda_1 x} + A_2 \left(1 + \frac{\lambda_2}{\bar{P}}\right) e^{\lambda_2 x} + A_3 \left(1 + \frac{\lambda_3}{\bar{P}}\right) e^{\lambda_3 x} \quad (20)$$

Appropriate boundary conditions are now required to be imposed to determine the unknown constants  $A_1$ ,  $A_2$  and  $A_3$ . The first boundary condition is that at  $x = 0$ ,  $u = 0$ , which leads to (from equation (18))

$$A_1 + A_2 + A_3 = 0 \quad (21)$$

The second boundary condition, that is,  $x = 0$ ,  $u_p = 0$  leads to (from equation (20))

$$\left(1 + \frac{\lambda_1}{\bar{P}}\right)A_1 + \left(1 + \frac{\lambda_2}{\bar{P}}\right)A_2 + \left(1 + \frac{\lambda_3}{\bar{P}}\right)A_3 = 0 \quad (22)$$

The third and the final boundary condition is that the ends of the PZT patch are stress free (Crawley and De Luis, 1987), which means that at  $x = l$  the strain  $u'_p$  is equal to the free piezoelectric strain  $\Lambda = d_{31}E_{31}$  (see equation (8c)). Hence, making use of equation (20) (after differentiation), we can derive

$$\left(1 + \frac{\lambda_1}{\bar{P}}\right)\lambda_1 e^{\lambda_1 l} A_1 + \left(1 + \frac{\lambda_2}{\bar{P}}\right)\lambda_2 e^{\lambda_2 l} A_2 + \left(1 + \frac{\lambda_3}{\bar{P}}\right)\lambda_3 e^{\lambda_3 l} A_3 = \Lambda \quad (23)$$

The constants  $A_1$ ,  $A_2$  and  $A_3$  can now be obtained by solving equations (21) to (23) simultaneously. Once determined, the constants can facilitate the determination of  $u$  and  $u_p$  at  $x = l$ , from which the equivalent mechanical impedance (with due consideration of shear lag effect), can be determined as (Bhalla et al., 2009b; Bhalla and Soh, 2004c)

$$Z_{eq} = Z_s \frac{u(x=l)}{u_p(x=l)} \quad (24)$$

which, when used in equation (1), in place of  $Z_s$ , facilitates deriving admittance signatures for adhesively bonded PZT patch for 1D case. The next section extends the formulations to 2D case, suitable for the 2D effective impedance model of Bhalla and Soh (2004a, 2004b).

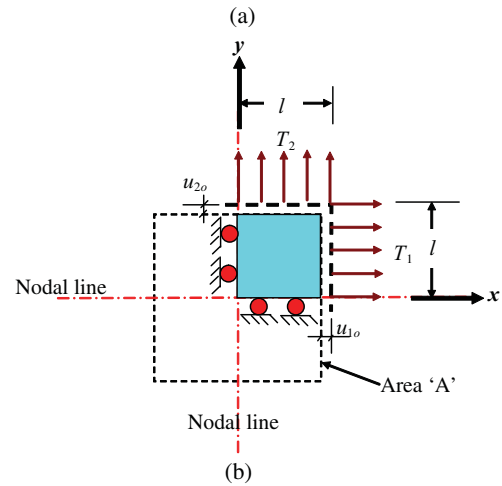
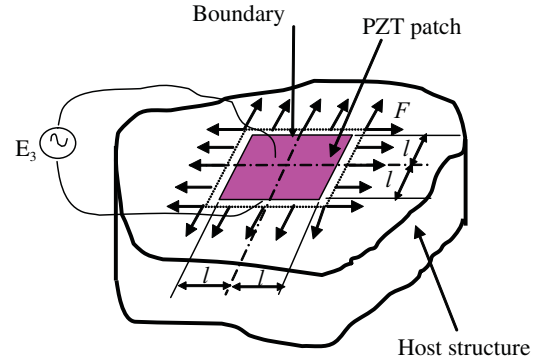


**Figure 5.** Effective impedance model (Bhalla and Soh, 2004a): (a) a PZT patch bonded to a host structure and (b) 2D effective interactions between PZT patch and host structure along the boundary.

2D: two-dimensional; PZT: lead zirconate titanate.

## 2D extension of refined shear lag formulations

Bhalla and Soh (2004a) introduced the concept of ‘effective mechanical impedance’ and coined the term ‘effective velocity’ as an alternative to ‘drive point velocity’ used previously. Effective impedance is based on the premise that the transmission of force between the PZT patch and host structure occurs along the 2D peripheral boundary of the patch bonded to the structure. Figure 5(a) shows the stresses acting along the boundary of the PZT patch bonded to a structure. For this configuration, the ‘effective mechanical impedance’ of the PZT patch can be defined as

$$Z_{a,eff} = \frac{\oint_S \vec{f} \cdot \hat{n} ds}{\dot{u}_{eff}} = \frac{F_{eff}}{j\omega u_{eff}} \quad (25)$$

where  $\hat{n}$  is a unit vector normal to the boundary and ‘ $F_{eff}$ ’ represents the effective peripheral force due to PZT patch’s deformation.  $u_{eff} = \delta A/P_0$  is the effective

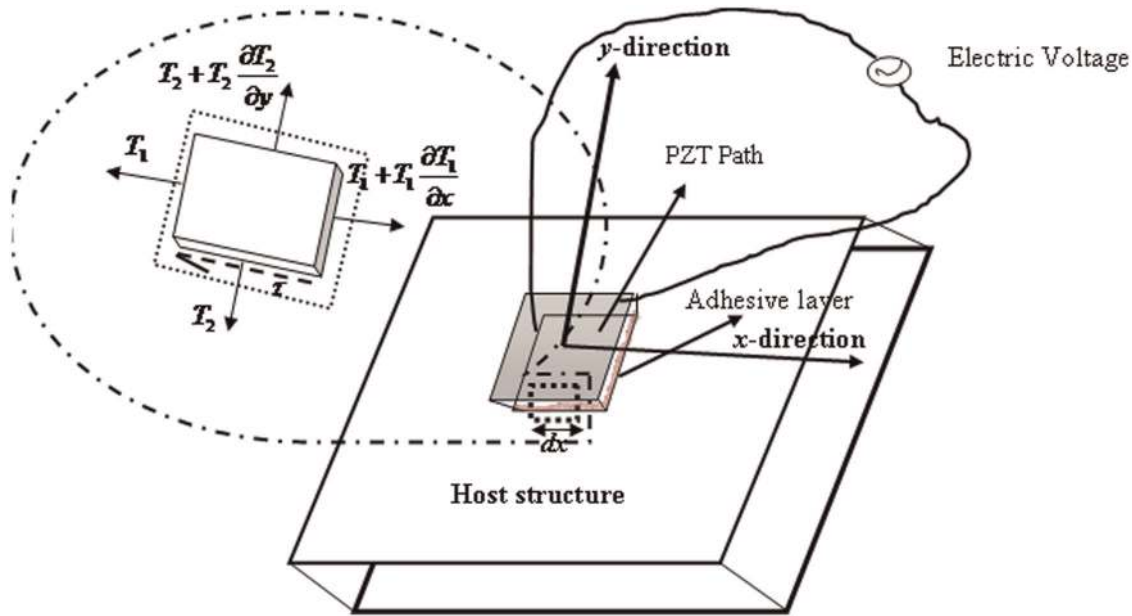


**Figure 6.** 2D schematic view of PZT–structure interaction model. 2D: two-dimensional; PZT: lead zirconate titanate.

displacement, with  $\delta A$  equal to the change in the patch's area and  $P_0$  is its perimeter in the undeformed condition. Due to symmetry, considering only one quarter of the PZT patch (as shown in Figure 5(b)), the effective displacement of the PZT patch can be simplified as

$$u_{eff} = \frac{\delta A}{P_0} = \frac{u_{1o}l + u_{2o}l + u_{1o}u_{2o}}{2l} \approx \frac{u_{1o} + u_{2o}}{2} \quad (26)$$

where  $u_{1o}$  and  $u_{2o}$  are the edge displacements (see Figure 5(b)). Consecutively, effective velocity can be expressed as

$$\dot{u}_{eff} = j\omega u_{eff} \quad (27)$$

With this definition, the following expression was derived by Bhalla and Soh (2004b) for

$$Z_{a,eff} = \frac{2h\bar{Y}^E}{j\omega(1-\nu)\bar{T}} \quad (28)$$

where  $\nu$  is the Poisson's ratio of the patch, and the term  $\bar{T}$  is given by

$$\bar{T} = \frac{1}{2} \left( \frac{\tan C_1 kl}{C_1 kl} + \frac{\tan C_2 kl}{C_2 kl} \right) \quad (29)$$

where  $C_1$  and  $C_2$  are the peak correction factors to be determined experimentally. The mechanical impedance of structure ( $Z_{s,eff}$ ) can be similarly defined, by applying a distributed effective force along the proposed boundary of the PZT patch. The final expression for admittance for 2D case derived by Bhalla and Soh (2004b) was

$$\bar{Y} = \frac{\bar{I}}{\bar{V}} = G + Bj = 4\omega j \frac{l^2}{h} \left[ \frac{\bar{T}}{\epsilon_{33}^T} - \frac{2d_{31}^2 \bar{Y}^E}{(1-\nu)} + \frac{2d_{31}^2 \bar{Y}^E}{(1-\nu)} \left( \frac{Z_{a,eff}}{Z_{s,eff} + Z_{a,eff}} \right) \bar{T} \right] \quad (30)$$

Equation (30) is considered in the refined shear lag model to derive the expression for admittance signature for 2D case. The instantaneous voltage  $\bar{V}$  across the PZT patch can be expressed as  $\bar{V} = V_0 e^{j\omega t}$  ( $V_0$  being the peak sinusoidal voltage). For EMI technique, the PZT patches are excited by very low voltage (usually less than 1 V<sub>rms</sub>) to generate suitable excitation in the host structure (Park et al., 2000a, 2000b, Park and Inman, 2007; Sun et al., 1995). Hence, for the current analysis, the value of  $V_0$  is taken as 1.41 V (which gives a root mean square (rms) value of 1 V).

The 2D equilibrium equations (similar to equation (2) for 1D case) deduced from the free body diagram (see Figure 6) can be expressed as follows (De Faria, 2003; Zhou et al., 1996)

$$\frac{\partial T_1}{\partial x} - \frac{\tau_{zx}}{h_p} = \rho \ddot{u}_{px} \quad (31)$$

and

$$\frac{\partial T_2}{\partial y} - \frac{\tau_{zy}}{h_p} = \rho \ddot{u}_{py} \quad (32)$$

where  $u_{px}$  and  $u_{py}$ , and  $T_1$  and  $T_2$  are the displacements and axial stresses on PZT patch along x- and y-directions, respectively. From 2D PZT–structure

constitutive relations (Bhalla and Soh 2004a, 2004c), the stress  $T_1$  along  $x$ -axis can be expressed as

$$T_1 = \frac{\bar{Y}E}{(1 - \nu^2)} [S_1 + \nu S_2 - \Lambda(1 + \nu)] \quad (33)$$

where  $S_1$  and  $S_2$  are the strains along  $x$ - and  $y$ -axes, respectively. Making note of the fact that  $S_1 = u'_{px}$ , and differentiating with respect to  $x$ , we get

$$\frac{\partial T_1}{\partial x} = \frac{\bar{Y}E}{(1 - \nu^2)} u''_{px} \quad (34)$$

Substituting equations (34), (8b) and (8d) into equation (31), and solving, we get

$$\frac{\bar{Y}E}{(1 - \nu^2)} u''_{px} - \frac{\bar{G}_s}{h_p h_s} (u_{px} - u_x) = -\rho \omega^2 u_{px} \quad (35)$$

which can be further reduced as

$$\bar{\alpha} u_{px} - u_x = \frac{1}{q_{eff}} u''_{px} \quad (36)$$

where

$$q_{eff} = \frac{G_s(1 - \nu^2)}{Y^E h_p h_s} \quad (37)$$

which is the 2D equivalent of the shear lag parameter  $q$  for 1D. Similarly, using equation (32), the equation for  $y$ -direction can be written as

$$\bar{\alpha} u_{py} - u_y = \frac{1}{q_{eff}} u''_{py} \quad (38)$$

Adding equations (36) and (38) and dividing by 2, we get

$$\bar{\alpha} \left( \frac{u_{px} + u_{py}}{2} \right) - \left( \frac{u_x + u_y}{2} \right) = \frac{1}{q_{eff}} \left( \frac{u''_{px} + u''_{py}}{2} \right) \quad (39)$$

Making use of the definition of effective displacement (Bhalla and Soh, 2004a), this can be expressed in a compact form as

$$\bar{\alpha} u_{(p,eff)} - u_{eff} = \frac{1}{q_{eff}} u''_{(p,eff)} \quad (40)$$

The second governing 2D shear lag equation (equivalent to equation (14) for 1D case), can similarly be derived, using the concept of effective displacement, as

$$\left( \frac{u_{px} + u_{py}}{2} \right) = \left( \frac{u_x + u_y}{2} \right) + \frac{\left( \frac{u'_x + u'_y}{2} \right)}{\bar{p}_{eff}} \quad (41)$$

or

$$u_{p,eff} = u_{eff} + \frac{u'_{eff}}{\bar{p}_{eff}} \quad (42)$$

where

$$\bar{p}_{eff} = -\frac{2l\bar{G}_s(1 + \nu)}{Z_{eff} j \omega h_s} \quad (43)$$

where  $\bar{p}_{eff}$  is the equivalent 2D shear lag parameter (Bhalla and Soh, 2004c)

Equation (43) is the second equivalent 2D shear lag parameter. Combining equations (40) and (42) as in the 1D case and solving, the governing differential equation results, as

$$u'''_{eff} + \bar{p}_{eff} u''_{eff} - \alpha q_{eff} u'_{eff} + (1 - \bar{\alpha}) \bar{p}_{eff} q_{eff} u_{eff} = 0 \quad (44)$$

For solving the above homogenous equation, its characteristic equation can be written as

$$\lambda^3 + \bar{p}_{eff} \lambda^2 - \alpha \bar{q}_{eff} \lambda + (1 - \alpha) \bar{p}_{eff} q_{eff} = 0 \quad (45)$$

Now, this expression is similar to the polynomial equation with complex coefficients for the 1D analysis (see equation (17)), but the parameters represent 2D interaction. It has three roots  $\lambda_1$ ,  $\lambda_2$ , and  $\lambda_3$  as for the 1D case. The final solution for  $u_{eff}$  and  $u_{p,eff}$  is similar to the 1D case with same boundary conditions. The equivalent effective impedance ( $Z_{s,eq,eff}$ ) for 2D refined shear lag model can thus be determined as

$$Z_{s,eq,eff} = Z_{s,eff} \left( \frac{u_{eff}(x=l)}{u_{p,eff}(x=l)} \right) \quad (46)$$

The above 2D shear lag-based impedance term can be directly used in equation (30) using  $Z_{s,eq,eff}$  in place of  $Z_{s,eff}$  to obtain the admittance signature duly considering the shear lag effect.

The new formulations derived above were compared with the results published by Bhalla and Soh (2004b, 2004c). The test structure consisted of an aluminium block (grade Al 6061 T6), 48 mm × 48 mm × 10 mm in size, instrumented with a PZT patch of size 10 mm × 10 mm × 0.3 mm (grade PIC 151; PI Ceramic, 2003), as shown in Figure 7(a). Table 1 lists the key physical parameters of the PZT patch, the aluminium block and the adhesive, considered while deriving the theoretical signatures. Figure 7(b) shows the 3D finite element model of a quarter of the test structure (Bhalla and Soh, 2004b), developed to determine the effective impedance,  $Z_{s,eff}$ , for use in deriving the theoretical signatures.  $Z_{s,eff}$  was obtained by applying a distributed harmonic force along the boundary of the PZT patch (see Figure 7(b)), carrying out dynamic harmonic analysis, and obtaining the effective displacement  $u_{eff}$ , from which  $Z_{s,eff}$  was obtained as the ratio of the effective force to the effective velocity (see equation (25)). The

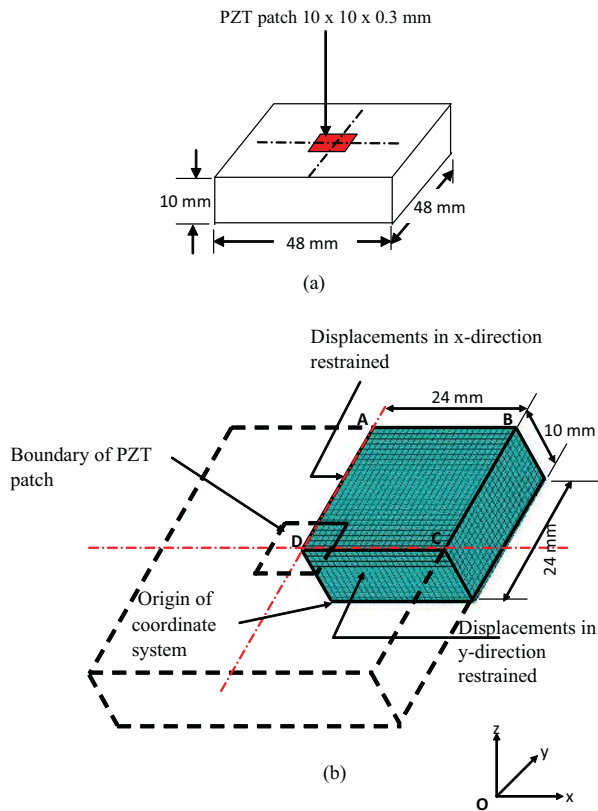


**Figure 7.** (a) Aluminium block structure and (b) finite element model of a quarter of structure. PZT: lead zirconate titanate.

**Table 1.** Parameters of PZT patch, aluminium block and adhesive bond.

| Material        | Physical parameter                                      | Value                   |
|-----------------|---|-------------------------|
| PZT patch       | Electric permittivity $\epsilon_{33}^T$ (F/m)           | $1.7785 \times 10^{-8}$ |
|                 | Peak correction factor ( $C_1, C_2$ )                   | 0.898                   |
|                 | $k = \frac{2d_{31}^2 \gamma^E}{(1-\nu)} (\text{N/V}^2)$ | $5.35 \times 10^{-9}$   |
|                 | Mechanical loss factor $\eta$                           | 0.0325                  |
|                 | Dielectric loss factor $\delta$                         | 0.0224                  |
| Aluminium block | Young's modulus (GPa)                                   | 68.95                   |
|                 | Density ( $\text{Kg m}^{-3}$ )                          | 2715                    |
|                 | Poisson's ratio $\nu$                                   | 0.33                    |
|                 | Rayleigh's damping coefficients                         |                         |
|                 | $\alpha$  | 0                       |
|                 | $\beta$   | $3 \times 10^{-9}$      |
| Adhesive        | Shear modulus ( $G_s$ ) (GPa)                           | 1                       |
|                 | Mechanical loss factor $\eta'$                          | 0.1                     |

PZT: lead zirconate titanate.

equivalent effective impedance (taking into consideration the shear lag effect as per the new refined model) was obtained using equation (46). A bond layer thickness of 0.125 mm was considered with  $G_s = 1$  GPa and the related mechanical loss factor  $\eta'$  as 10%,

respectively. Figures 8 and 9 show a comparison of the plots of conductance ( $G$ ) and susceptance ( $B$ ), respectively, obtained using present model, over a frequency range 0–200 kHz with those obtained using the previous model (Bhalla and Soh, 2004c). It can be observed that using the new refined model, the peaks of both the conductance as well as susceptance plots are lower than the predictions of the previous model, a consequence of the inclusion of the inertial effects. This can be more appreciated by the graph shown in part (b) of Figures 8 and 9, where the focus is near the resonance peaks. The slope of the susceptance plot (Figure 9) also gets lowered. Figure 10 compares signatures of the three models, that is, Liang et al., (1994), Bhalla and Soh (2004c) and the present refined model. As expected, the prediction of Liang's model, which takes 1D interaction into account, is drastically different from the other two models.

Figures 11 and 12 compare the analytical and experimental conductance and susceptance signatures for two different bond thickness ratio ( $h_s/h_p = 0.417$ ) and ( $h_s/h_p = 0.834$ ), respectively. Since here the PZT patches are of different thicknesses (0.3 mm and 0.15 mm, respectively), normalized values, that is,  $Gh/l^2$  and  $Bh/l^2$  are compared rather than the absolute values. The refined model eliminates a downward peak around 198 kHz predicted by the previous model (see Figure 11(b)). The peaks of both conductance and susceptance plots are much lower when computed using refined model. From these comparisons, it can be observed that the present model is qualitatively much better match with experimental observations. This is because of the more accurate modelling and involvement of the inertia term.

### Effect of inclusion of adhesive mass

After properly accounting for inertia effect of PZT patch, this section goes one step further to include the mass of adhesive (in term  $dm$  of equation (2)) so far not considered in any previous approach. After considering the mass of the adhesive, the inertial term of equation (2) can be rewritten as

$$I = dm_p \ddot{u}_p + dm_s \ddot{u}_s \quad (47)$$

where  $dm_p$  and  $dm_s$  are the differential masses of the PZT patch and the adhesive, respectively, and  $dm_p$  and  $dm_s$  are the corresponding velocities.

Furthermore

$$dm_p = \rho w h_p \quad (48a)$$

$$dm_s = \rho_s w h_s \quad (48b)$$

$$\ddot{u}_p = -\omega^2 u_p \quad (48c)$$

$$\ddot{u}_s = -\omega^2 \left( \frac{u_p + u}{2} \right) \quad (48d)$$

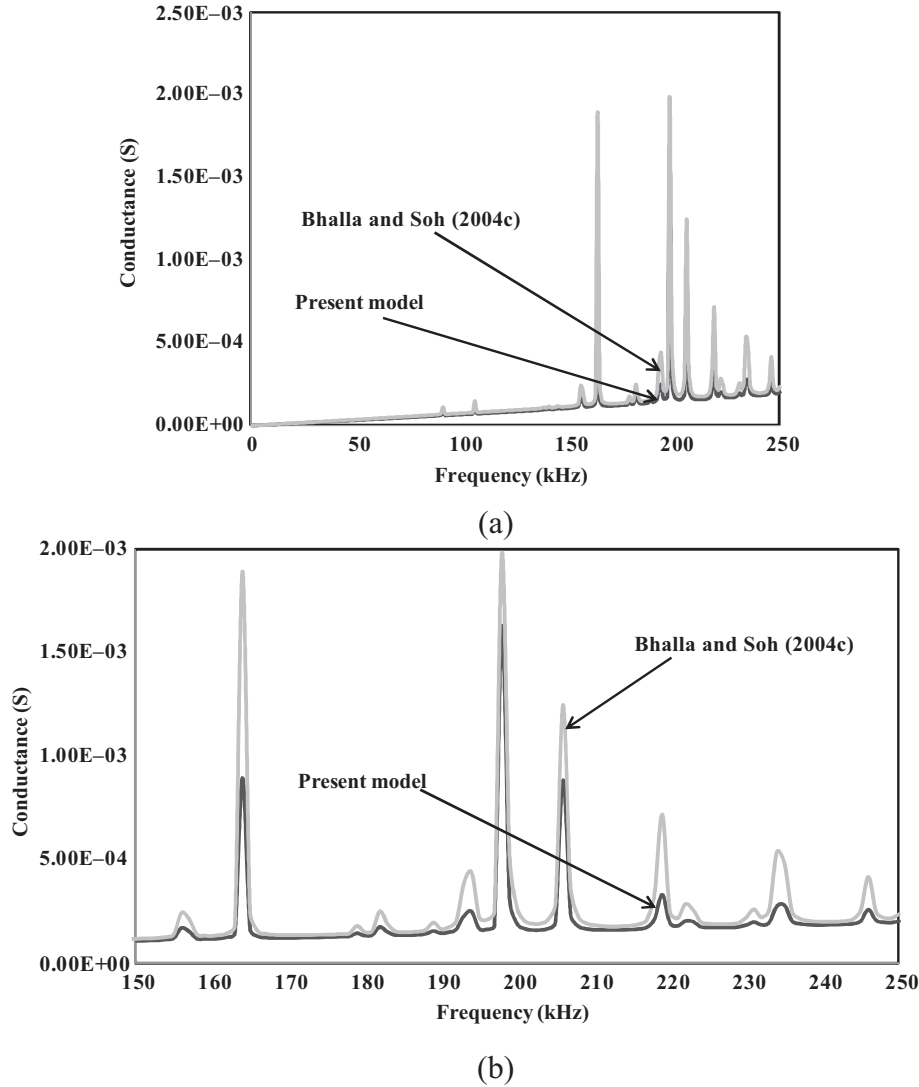


**Figure 8.** Comparison of conductance signature with previous analytical model (Bhalla and Soh, 2004c): (a) plot in 0–250 kHz range and (b) closer view in 150–250 kHz range.

where  $\rho_s$  is the density of the adhesive. It may be noted from equation (48d) that average velocity has been considered for the adhesive layer, assuming a linear variation from  $u$  (at the surface of host structure) to  $u_p$  (at the bottom of the PZT patch, as can be seen from Figure 2). With above substitutions, equation (9) can be modified as

$$\left[ 1 - \frac{\rho h_p h_s \omega^2}{G_s} - \frac{\rho_s h_s^2 \omega^2}{2G_s} \right] u_p - \left[ 1 + \frac{\rho_s h_s^2 \omega^2}{2G_s} \right] u = \frac{1}{q} u_p'' \quad (49)$$

In compact form, we can write

$$\bar{\alpha}' u_p - \bar{\beta} u = \frac{1}{q} u_p'' \quad (50)$$

where  $\bar{\alpha}'$  is the modified inertia parameter (see equation (10a)), given by

$$\bar{\alpha}' = 1 - \frac{\left( \rho h_p + \frac{\rho_s h_s}{2} \right) h_s \omega^2}{G_s} \quad (51)$$

and  $\bar{\beta}$  is the second inertia parameter, given by

$$\bar{\beta} = 1 + \frac{\rho_s h_s^2 \omega^2}{2G_s} \quad (52)$$

Similarly, for the case of 2D effective impedance, equation (35) can be reformed for  $x$ -direction as

$$\frac{\bar{Y}^E}{(1 - \nu^2)} u_{px}'' - \frac{\bar{G}_s}{h_p h_s} (u_{px} - u_x) = -\rho \omega^2 u_{px} - \rho_s \omega^2 \left( \frac{u_{px} + u_x}{2} \right) \quad (53)$$

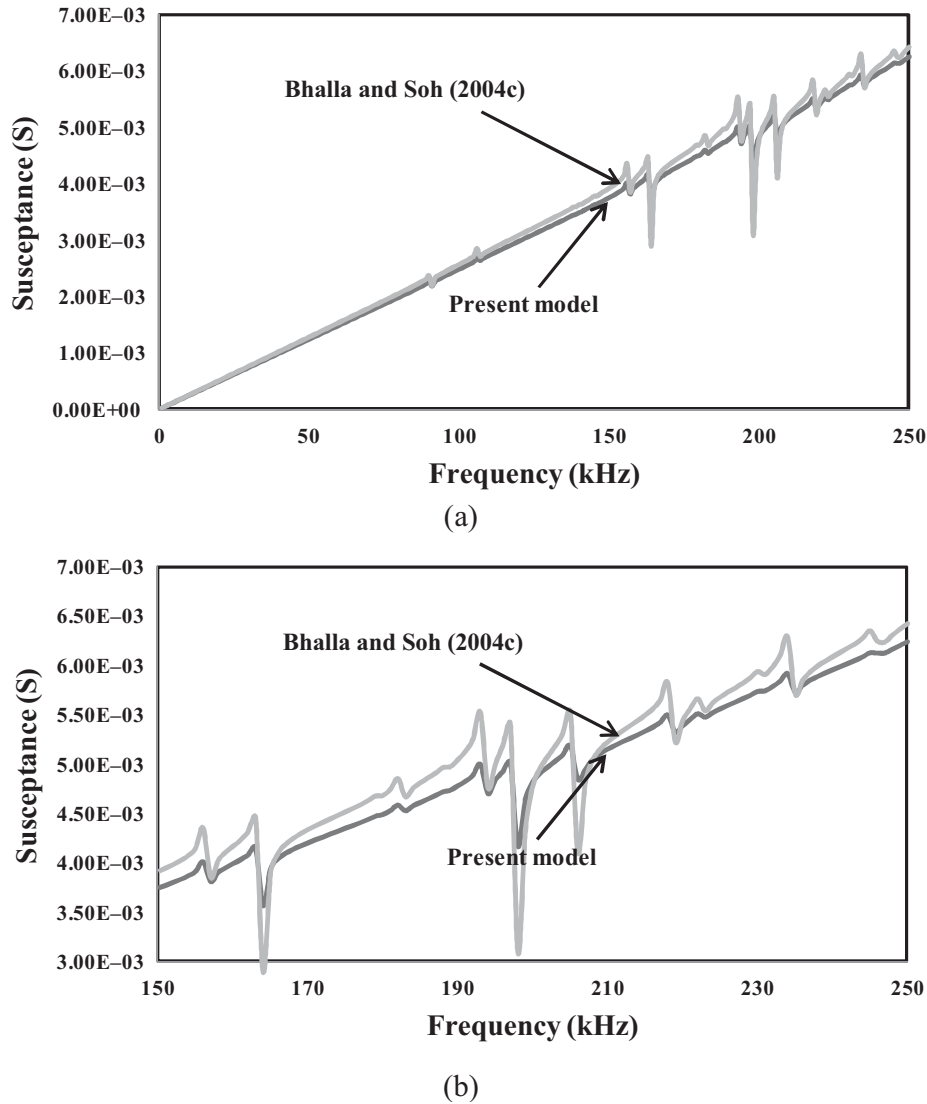


**Figure 9.** Comparison of susceptance signature with previous analytical model (Bhalla and Soh, 2004c): (a) plot in 0–250 kHz range and (b) closer view in 150–250 kHz range.

Hence, equation (40) can be modified as

$$\left[ \frac{1 - \frac{\rho h_p h_s \omega^2}{G_s} - \frac{\rho_s h_p h_s \omega^2}{2G_s} \right] u_{p,eff} - \left[ 1 + \frac{\rho_s h_p h_s \omega^2}{2G_s} \right] u_{eff} = \frac{1}{q_{eff}} u''_{p,eff} \quad (54)$$

$$\overline{\alpha'}_{eff} u_{p,eff} - \overline{\beta}_{eff} u_{eff} = \frac{1}{q_{eff}} u''_{p,eff} \quad (55)$$

where  $q_{eff}$  is given by equation (37) and  $\overline{\alpha'}_{eff}$  and  $\overline{\beta}_{eff}$  are redefined for the 2D case as

$$\overline{\alpha'}_{eff} = \left( 1 - \frac{(\rho + \frac{\rho_s}{2}) \omega^2 h_p h_s}{G_s} \right) \quad (56a)$$

$$\overline{\beta}_{eff} = \left( 1 + \frac{\rho_s \omega^2 h_p h_s}{2G_s} \right) \quad (56b)$$

The second governing equation of shear lag, namely, equation (42) will remain unchanged. Combining equations (42) and (55), eliminating the  $u_{p,eff}$ , we can obtain the modified governing differential equation as

$$u'''_{eff} + \overline{p}_{eff} u''_{eff} - \overline{\alpha'}_{eff} q_{eff} u'_{eff} + (\overline{\alpha'}_{eff} - \overline{\beta}_{eff}) \overline{p}_{eff} q_{eff} = 0 \quad (57)$$

Repeating the same procedure (with similar characteristic equation and boundary conditions) to solve the homogenous equation as it was done in the 1D and 2D case of previous sections, equation (57) can be solved. Figure 13 shows the plots of  $G$  and  $B$  based on above considerations for  $h_s = 0.125$  mm and compare them with those obtained by neglecting the adhesive mass. On close inspection, it can be observed that the inclusion of the adhesive mass leads to further lowering of the peaks of  $G$  and  $B$  and also the overall slopes of  $B$

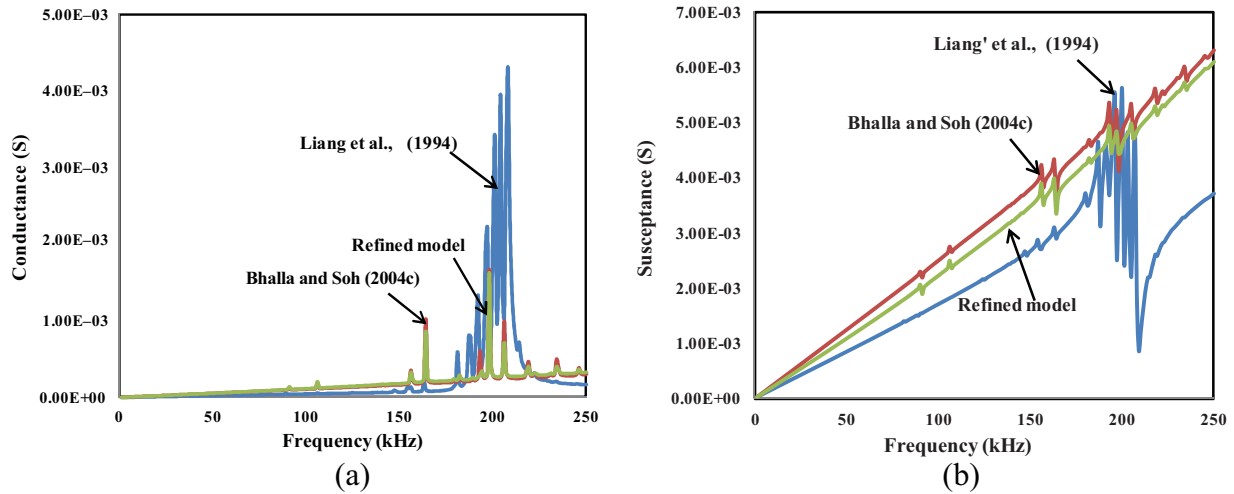


**Figure 10.** Comparison of refined admittance signature with previous analytical model (Bhalla and Soh, 2004c) and Liang et al. (1994). (a) Conductance vs frequency and (b) susceptance vs frequency.

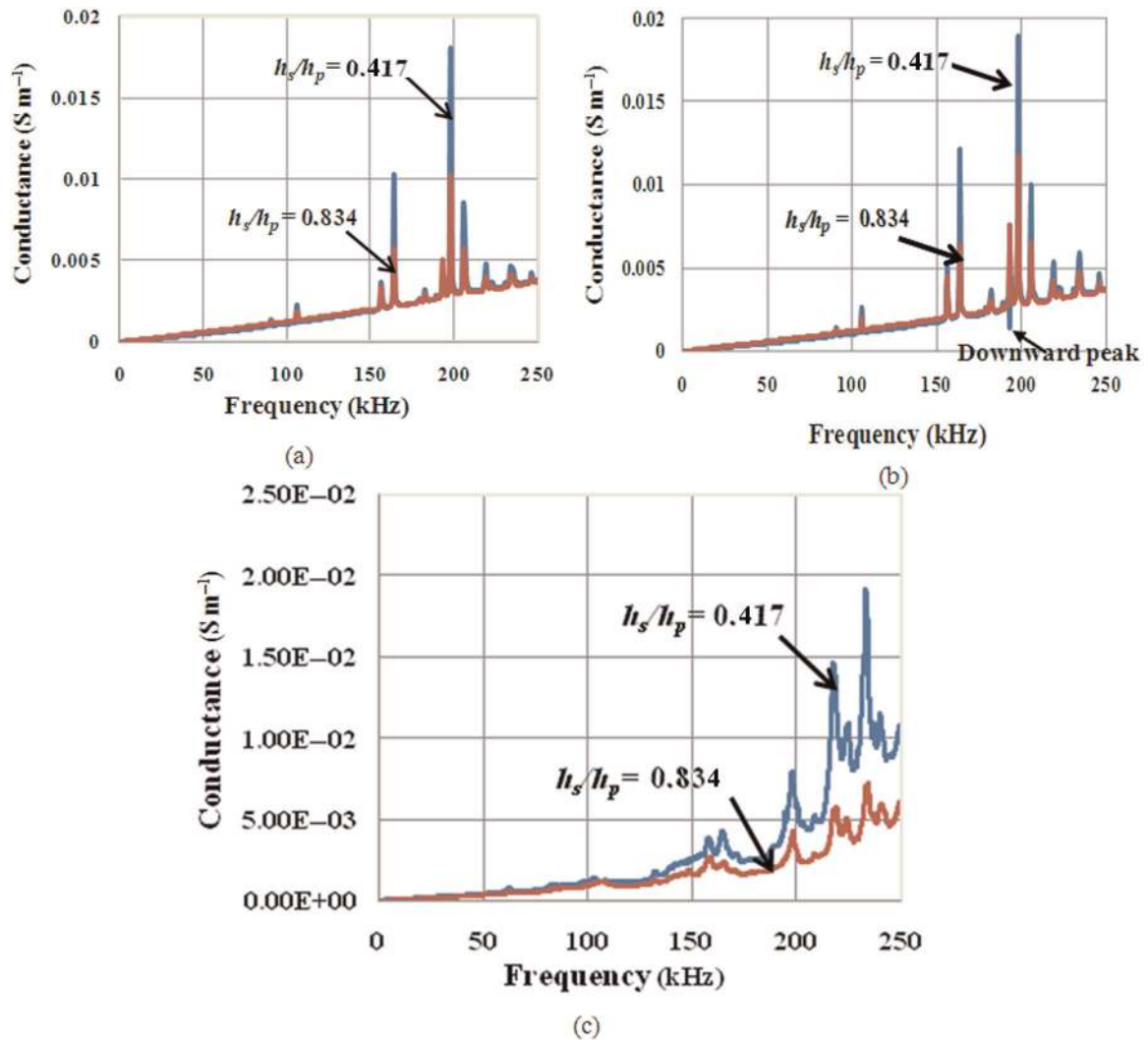


**Figure 11.** Comparison of conductance of experimental data (Bhalla and Soh, 2004c) with proposed model: (a) normalized analytical conductance (Refined model) for  $h_s/h_p = 0.417$  and  $h_s/h_p = 0.834$ , (b) normalized analytical conductance (Bhalla and Soh, 2004c) for  $h_s/h_p = 0.417$  and  $h_s/h_p = 0.834$  and (c) normalized experimental conductance (Bhalla and Soh, 2004c) for  $h_s/h_p = 0.417$  and  $h_s/h_p = 0.834$ .

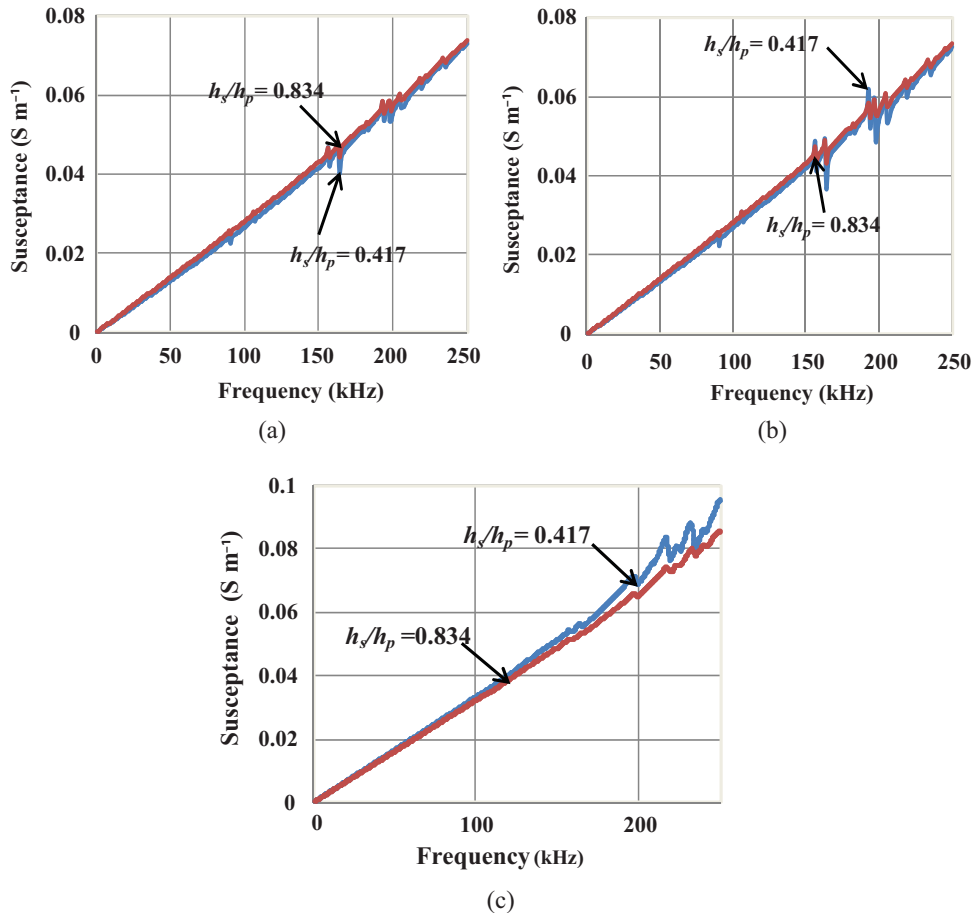


**Figure 12.** Comparison of susceptance of experimental data (Bhalla and Soh, 2004c) with proposed model: (a) normalized analytical susceptance (refined model) for  $h_s/h_p = 0.417$  and  $h_s/h_p = 0.834$ , (b) normalized analytical susceptance (Bhalla and Soh, 2004c) for  $h_s/h_p = 0.417$  and  $h_s/h_p = 0.834$  and (c) normalized experimental susceptance (Bhalla and Soh, 2004c) for  $h_s/h_p = 0.417$  and  $h_s/h_p = 0.834$ .

slightly. However, at the same time, it can also be noted that neglecting the mass of the adhesive will not make as significant difference as neglecting the inertia term. Hence, the mass of the adhesive can possibly be ignored.

### Shear stress profile in bond layer

This section investigates the distribution of the shear stress within the bond layer, using the refined model developed in this article. The shear stresses cannot be measured experimentally for the minutely thick PZT-adhesive-structure system. Hence, analytical approach or finite element approach are the only possible avenues for stress analysis. In this investigation, equation (8d) is employed, by replacing  $u_p$  and  $u$  by  $u_{p,eff}$  and  $u_{eff}$ , respectively. For simplicity, the inertia term associated with the adhesive is ignored. Figure 14 shows the plot of the interfacial shear stress as a function of distance, from  $x = 0$  to  $x = l$  at a frequency of 91 kHz (first resonance peak). It should be noted that this plots only the absolute values. From the plot, it can be observed that the stress is zero at  $x = 0$ , increases to

the maximum value and then remains constant. Figure 15 similarly shows a plot of the effective strain ( $u'_{p,eff}$ ) in the PZT patch along the length. The variation is similar to that of shear stress (Figure 13). The stresses in the two principal directions in the PZT patch can be expressed as

$$T_1 = \frac{\overline{Y}E}{(1-\nu^2)} [(u'_{px} + \nu u'_{py}) - \Lambda(1+\nu)] \quad (58)$$

$$T_2 = \frac{\overline{Y}E}{(1-\nu^2)} [(u'_{py} + \nu u'_{px}) - \Lambda(1+\nu)] \quad (59)$$

Adding equations (58) and (59) and dividing by 2, we get

$$T_{eff} = \frac{(T_1 + T_2)}{2} = \frac{\overline{Y}E}{(1-\nu)} [u'_{p,eff} - \Lambda] \quad (60)$$

Figure 16 shows a plot of  $T_{eff}$  as a function of  $x$  for the PZT-adhesive-aluminium block system at a frequency of 91 kHz. From Figure 16, it can be noted that the effective axial stress is maximum at the centre of the

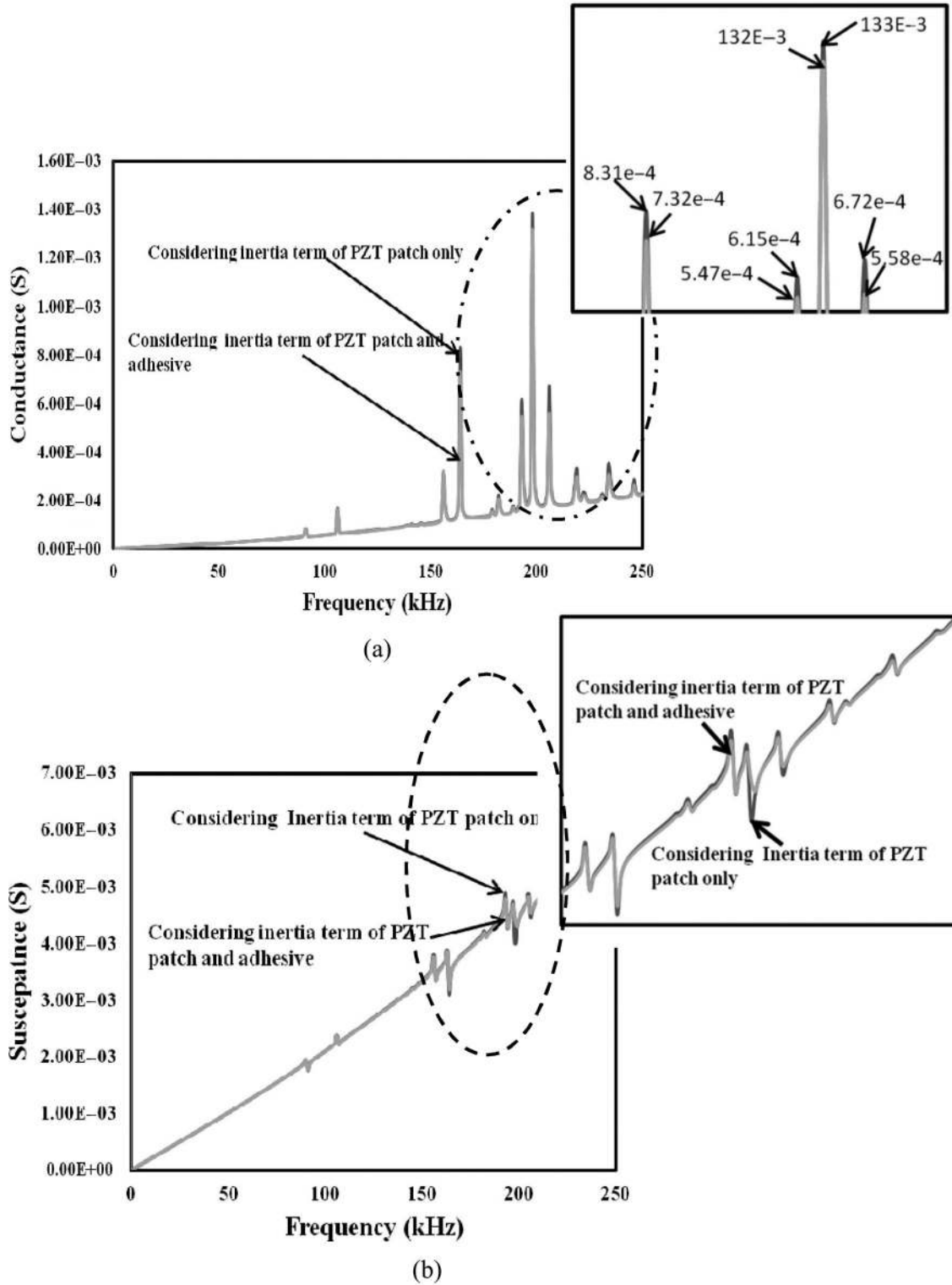


**Figure 13.** Effect of mass of adhesive on signatures: (a) conductance (b) susceptance. PZT: lead zirconate titanate.

patch and reduces to zero at the ends. The area under the curve normalized with respect to  $T_{eff}l$  will result in a parameter similar to the effective length ratio defined

by Sirohi and Chopra (2000) for the sensor case. In the present analysis, however, both sensor and actuator effects have been simultaneously considered.

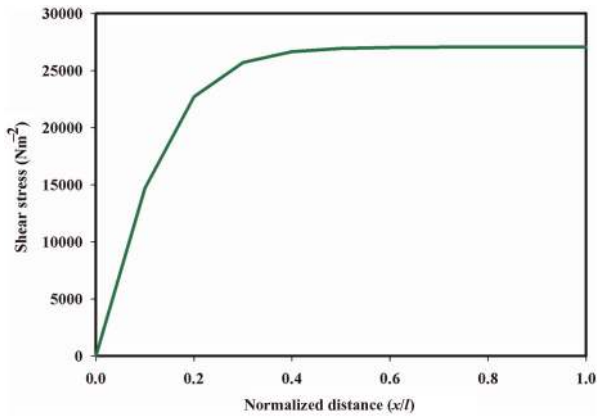


Figure 14. Variation of shear stress in bond layer.

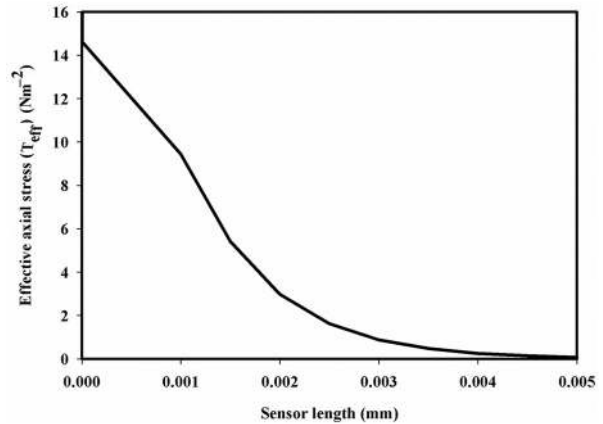


Figure 16. Variation of effective stress ( $T_{eff}$ ) over the length of PZT patch.  
PZT: lead zirconate titanate.

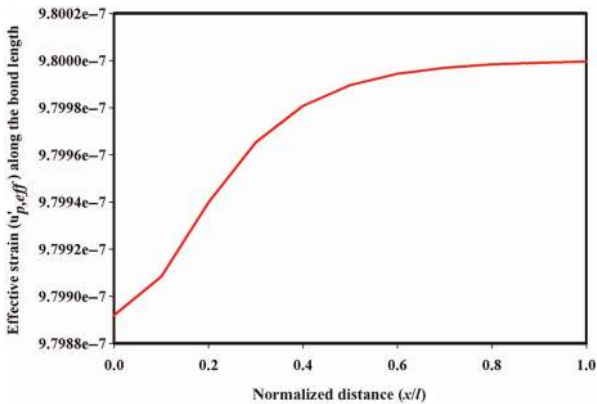


Figure 15. Profile of effective strain ( $T_{eff}$ ) over the length of PZT patch.  
PZT: lead zirconate titanate.

### Parametric study

This section studies the influence of various physical parameters on  $G$  and  $B$  with the aid of the new refined model presented in this article. The frequency range is limited to 0–250 kHz, since for most of the civil engineering applications (Soh et al., 2000), a sub-range within 0–250 kHz is adequate. Again, for simplicity, the mass of adhesive is ignored for following parametric studies. Figure 17 shows the influence of the bond layer’s shear modulus of elasticity ( $G_s = 1, 0.5$  and  $0.05$  GPa) on the conductance and susceptance plots. It is observed that as  $G_s$  decreases, the peaks of both  $G$  and  $B$  subside down and the overall slope of  $B$  decreases. For very low value ( $G_s = 0.05$  GPa), the signature tends to be similar to that of the free PZT patch. The observations are very similar to the previous models. The influence of bond layer thickness is already covered in the previous section, as demonstrated by Figures 11 and 12. As apparent from these figures, the influence of increasing bond layer thickness is similar

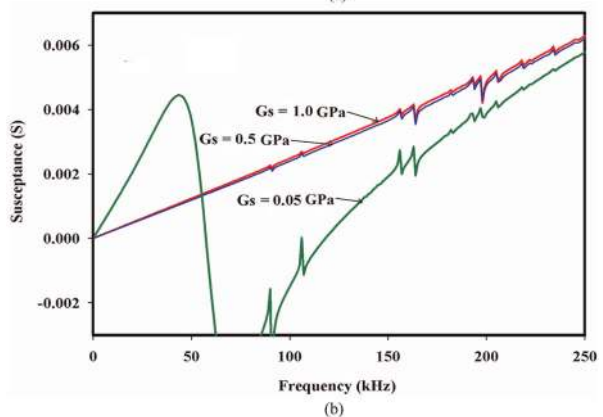
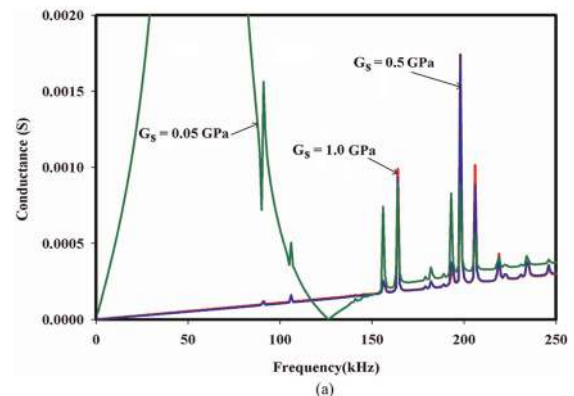
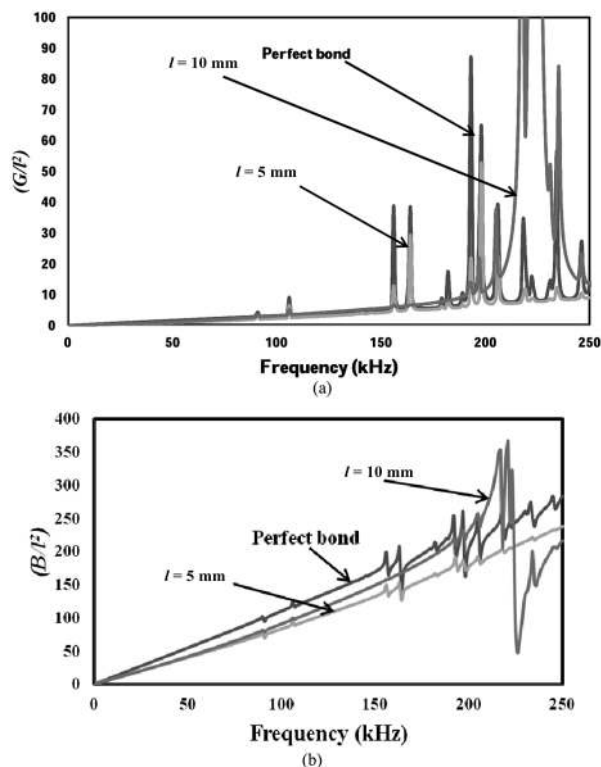
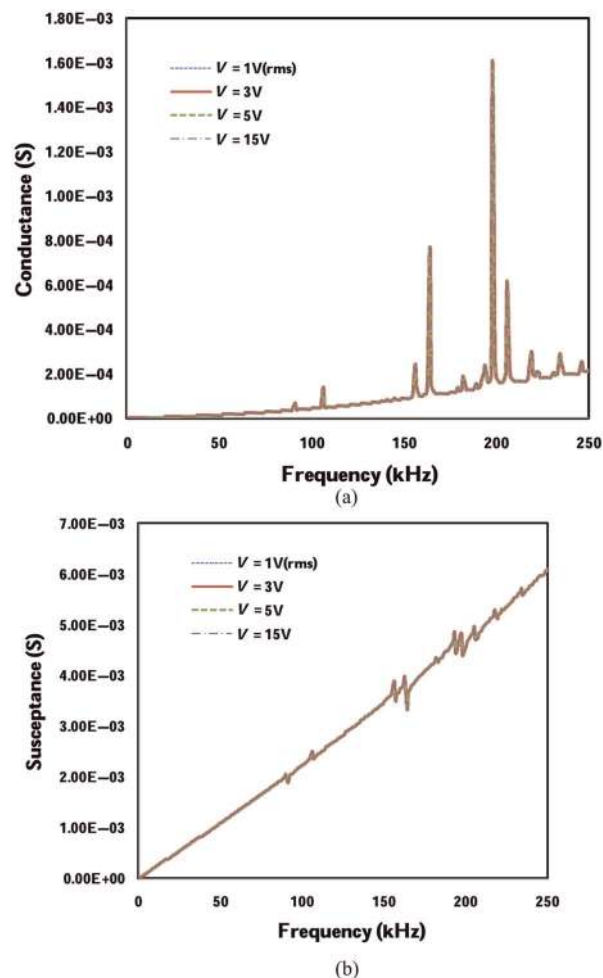


Figure 17. Influence of shear modulus of elasticity of bond layer on EMI signature: (a) conductance and (b) susceptance.  
EMI: electromechanical impedance.

to that of decreasing  $G_s$ . Figure 18 shows the influence sensor length on  $G$  and  $B$ . For the purpose of comparison, normalized values ( $G/l^2$ ) and ( $B/l^2$ ) have been plotted. It is observed that for small sensor length ( $l = 5$  mm), the signatures are closer to those for perfect bonding condition; however, the quality of signatures degrades for longer PZT patches ( $l = 10$  mm). Hence,



**Figure 18.** Influence of sensor length on EMI signature: (a) normalized conductance and (b) normalized susceptance. EMI: electromechanical impedance.



**Figure 19.** Influence of electric voltage on EMI signature: (a) conductance and (b) susceptance. EMI: electromechanical impedance.

smaller patches should be preferred over longer ones. This observation is also similar to the previous studies (Bhalla and Soh, 2004c). Figure 19 shows the influence of excitation voltage on present shear lag model. Electric potential has very negligible effect on shear lag model, as clearly evident from the Figure 19.

## Conclusion

This article has presented a rigorously refined new analytical model for considering shear lag effect in the EMI formulations. The treatment is complete in the sense that the model includes the inertial as well as the shear stress term simultaneously, a feature missing in the previous models. The results show that it is important to consider the inertia effect, which has significant influence on the signatures, especially in terms of lowering the peak values and the overall slope of conductance and susceptance. The effect of inclusion of the mass of adhesive has also been investigated. The results show that the mass of the adhesive play a negligible role and can be neglected. The distribution of shear stress and effective strain in the bond layer and the variation of axial stresses in the PZT patch have also been investigated for this article. Finally, a parametric study has also been conducted to study the influence of different parameters on conductance and susceptance signatures.

## Funding

This research received no specific grant from any funding agency in the public, commercial or not-for-profit sectors.

## References

- Abe M, Park G and Inman DJ (2002). Impedance-based monitoring of stress in thin structural members. In: Yuji M (ed.) *Proceeding of 11th international conference on adaptive structures and technologies*. Nagoya (Japan), CRC Press, pp. 285–292.
- Ayres JW, Lalande F, Chaudhry Z, et al. (1998) Qualitative impedance-based health monitoring of civil infrastructures. *Smart Materials and Structures* 7(5): 599–605.
- Bhalla S and Soh CK (2004a) Structural health monitoring by piezo-impedance transducers I: modelling. *Journal of Aerospace Engineering* 17(4): 154–165.
- Bhalla S and Soh CK (2004b) Structural health monitoring by piezo-impedance transducers II: applications. *Journal of Aerospace Engineering* 17(4): 166–175.
- Bhalla S and Soh CK (2004c) Impedance based modelling for adhesively bonded piezo-transducers. *Journal of Intelligent Material Systems and Structures* 15(12): 955–972.

- Bhalla S, Gupta A, Bansal S, et al. (2009a) Ultra low cost adaptations of electro-mechanical impedance technique for structural health monitoring. *Journal of Intelligent Material Systems and Structures* 20(8): 991–999.
- Bhalla S, Kumar P, Gupta A, et al. (2009b) Simplified impedance model for adhesively bonded piezo-impedance transducers. *Journal of Aerospace Engineering* 22(4): 373–382.
- Ceramic PI (2003) Available at: <http://www.piceramic.de>
- Crawley EF and De Luis J (1987) Use of piezoelectric actuators as elements of intelligent structures. *AIAA Journal* 25(10): 1373–1385.
- De Faria AR (2003) The effect of finite thickness bonding on the sensing effectiveness of piezoelectric patches. *Smart Materials and Structures* 12: N5–N8.
- Dugani R. (2009) Dynamic behaviour of structure-mounted disk-shape piezoelectric sensors including the adhesive layer. *Journal of Intelligent Material Systems and Structures* 20: 1553–1564.
- Liang C, Sun FP and Rogers CA (1994) Coupled electro-mechanical analysis of adaptive material systems – determination of the actuator power consumption and system energy transfer. *Journal of Intelligent Material Systems and Structures* 5: 12–20.
- Lim YY, Bhalla S and Soh CK (2006) Structural identification and damage diagnosis using self-sensing piezo-impedance transducers. *Smart Materials and Structures* 15(4): 987–995.
- Ong CW, Yang Y, Wong YT, et al. (2002) The effects of adhesive on the electro-mechanical response of a piezoceramic transducer coupled smart system. In: *Proceedings of the ISSS-SPIE international conference on smart materials, structures and systems*, IISc, Bangalore, Karnataka, India, 12–14 December, pp. 191–197.
- Overly TGS, Park G, Farinholt Kevin M, et al. (2008) Development of extremely compact impedance-based wireless sensing device. *Smart Materials and structures* 17: 1–9.
- Park G and Inman DJ (2007) Structural health monitoring using piezoelectric impedance measurements. *Philosophical Transaction of Royal Society A* 365: 373–392.
- Park G, Cudney HH and Inman DJ (2000a) Impedance-based health monitoring of civil structural components. *Journal of Infrastructures Systems* 6: 153–160.
- Park G, Cudney HH and Inman DJ (2000b) An integrated health monitoring technique using structural impedance sensors. *Journal Intelligent Material Systems and Structures* 11: 448–455.
- Park S, Yun CB, Roh Y, et al. (2006) PZT-based active damage detection techniques for steel bridge components. *Smart Materials and Structures* 15(4): 957–966.
- Qing XP, Chan HL, Beard SJ, et al. (2006) Effect of adhesive on performance of piezoelectric elements used to monitor structural health. *International Journal of Adhesion and Adhesives* 26(8): 622–628.
- Shanker R, Bhalla S and Gupta A (2011) Dual use of PZT Patches as sensors in global dynamic and local EMI techniques for structural health monitoring. *Journal of Intelligent Material Systems and Structures* 22(16): 1841–1856.
- Sirohi J and Chopra I (2000) Fundamental understanding of piezoelectric strain sensors. *Journal of Intelligent Material Systems and Structures* 11(4): 246–257.
- Soh CK, Tseng KKH, Bhalla S, et al. (2000) Performance of smart piezoceramic patches in health monitoring of a RC Bridge. *Smart Materials and Structures* 9(4): 533–542.
- Sun FP, Chaudry Z, Rogers CA, et al. (1995) Automated real-time structure health monitoring via signature pattern recognition. In: *Proceedings of SPIE*, San Diego, CA, 27 February–1 March, pp. 236–247. SPIE.
- Wang J and Zeng S (2008) Enhanced interface stress analysis of piezoelectric smart beams. *Smart Structure and Materials* 17: 1–12.
- Xu YG and Liu GR (2002) A modified electro-mechanical impedance model of piezoelectric actuator-sensors for debonding detection of composite patches. *Journal of Intelligent Material Systems and Structures* 13(6): 389–396.
- Zhou SW, Liang C and Rogers CA (1996) An impedance-based system modelling approach for induced strain actuator-driven structures. *Journal of Vibrations and Acoustics* 118(3): 323–331.